ChemComm

Electrochemically Induced Crystallization of Amorphous Materials in Molten MgCl2: Boron Nitride and Hard Carbon

Journal:	*ChemComm*
Manuscript ID	CC-COM-11-2019-008717.R1
Article Type:	Communication

COMMUNICATION

Electrochemically Induced Crystallization of Amorphous Materials in Molten $MgCl_2$: Boron Nitride and Hard Carbon

Received 00th January 20xx,
Accepted 00th January 20xx

DOI: 10.1039/x0xx00000x

Prashant Bagri,[a] Bishnu P. Thapaliya,[b] Zhenzhen Yang,[b] Wei Jiang,[b] Dino Sulejmanovic,[c] Huimin Luo,[d] and Sheng Dai*[a, b]

A novel and versatile strategy toward the amorphous-to-crystalline transformation of boron nitride (BN) with the capability to control the degree of crystallization was developed through an electrochemical pathway using $MgCl_2$ at low temperature (750 °C). This procedure can be extended to the transformation of amorphous carbon to graphite, which significantly reduce the energy, cost, and accelerates synthesis process and could potentially replace the industrial graphite synthesis globally. Thus, synthesized graphite exhibits much enhanced electrochemical performance at high charge-discharge rates (5C) compared to commercial synthetic graphite.

Boron nitride, in its disordered form, like carbon, can be categorized into soft and hard forms with respect to the ease with which they can be crystallized. As the names suggest, the soft forms can be crystallized by heat treatment, whereas the hard forms are resistant to crystallization and remain disordered. Hexagonal boron nitride (h-BN) is an exciting material that is documented to have excellent thermal and optical properties suitable for the application in the energy storage.[1-3] The properties of h-BN can vary depending on their characteristics like size, surface area, crystal defects etc.[1, 4-6]

h-BN is regarded as a graphene analog and commonly referred to as 'white graphene.' h-BN is reported to have a layered honeycomb-like structure consisting of alternating B and N atoms. Previously, the synthesis and transformation of amorphous BN to h-BN nanosheets was extremely challenging, requiring temperatures as high as 2000 °C[7, 8]. Fabrication of few layered h-BN nanosheets are mostly prepared via either a solid-phase mechanical method, liquid-phase exfoliation or gas exfoliation in liquid N_2. However, the obtained h-BN materials often suffer from low surface areas or low crystalline structures[9-12]. Only recently, our group reported a strategy for the transformation of amorphous h-BN to crystalline h-BN using Mg metal.[13] However, this molten metal flux approach requires stringent transformation conditions (900 °C) and can introduce potential impurities even with acid wash procedure after thermal treatment. In addition, liquid Mg metal is flammable and strict inert gas condition as well as a unique stainless-steel autoclave is required. Additionally, the metal flux approach does not provide the ability to control the reaction and achieve the desired degree of crystallization. Herein, we report a superior electrochemical approach that precludes the use of molten Mg metal and the safety hazards associated with it. We hypothesized whether it would be possible to generate Mg metal in-situ using molten $MgCl_2$, analogous to the previous processes with molten $CaCl_2$.[14, 15]

The essence of our strategy lies in the cathodic polarization of amorphous BN in molten $MgCl_2$ at 750 °C, resulting in the formation of highly ordered, crystalline flakes of h-BN. Furthermore, we validate the versatility of our electrochemical crystallization process by demonstrating the transformation of amorphous hard carbon to graphite with a high degree of graphitization.

The as-prepared amorphous BN was pelletized (0.2 g) and wrapped in Mo mesh (see ESI for details). This BN pellet-Mo mesh assembly was attached to a Mo rod (ESPI Metals) using Mo wires (Goodfellow USA), which served as the working electrode. Glassy carbon rods (6 mm, HTW Germany) served as counter electrodes for the electrochemical cell. A glassy carbon crucible containing $MgCl_2$ was placed in a sealed quartz reactor. The quartz reactor was heated using an electric furnace (The Mellen Company). $MgCl_2$ was dehydrated previously (See ESI for details). Amorphous carbon electrodes were prepared using the same procedure. The only difference was the use of Ni mesh to wrap the carbon pellet (0.5 g).

[a] Address here. a Chemical Science Division, Oak Ridge National Laboratory, 1 Bethel Valley Rd, Oak Ridge, Tennessee, 37831
[b] Department of Chemistry, University of Tennessee, Knoxville, Tennessee, 37916
[c] Materials Science and Technology Division, Oak Ridge National Laboratory, Oak Ridge, Tennessee 37831
[d] Energy and Transportation Science Division, Oak Ridge National Laboratory, Oak Ridge, Tennessee 37831, United States
E-mail: dais@ornl.gov

Electronic Supplementary Information (ESI) available: supplementary figures and experimental procedures. See DOI: 10.1039/x0xx00000x

After treatment in the molten salt, the corresponding pellet was crushed and leached in a mild acid (0.1 N HCl) for 24 hours. The product was further washed with deionized water and filtered to remove residual acid. It was subsequently dried in an oven at 120 °C for 24 hrs. For electrochemically generated graphite (EGCs), their battery performance was investigated in two-electrode coin cells with lithium metal as a counter/reference electrode. The slurry casting method was used to make the electrode. A slurry was prepared by mixing EGC, hard carbon (CB45), and PVDF (poly (vinylidene fluoride)) in a weight ratio of 90:4:6 in N-methyl pyrrolidone (NMP). The slurry was cast on the copper foil using a doctor blade. The loading of EGC was approximately 1.84 mg $cm^{2,}$ with the electrode area of 1.27 cm^2. 1.2 M lithium hexafluorophosphate ($LiPF_6$) in ethylene carbonate (EC) / diethyl carbonate (DEC) / dimethyl carbonate (DMC) in a 1:1:1 ratio by volume was used as electrolyte. Celguard 2325 (Celgard Inc., USA) was used as a separator between the two electrodes. The coin cells were assembled inside the high purity argon glove box (≤ 0.5 ppm O_2 and ≤ 0.5 ppm H_2O). The galvanostatic charge-discharge cycling was performed between 0.005 V to 3.0 V at room temperature at different current densities (0.1 C, 1C, and 5C, where 1 C = 372 mAh g^{-1}) to test the feasibility of EGCs as an anode for fast charging battery applications. Cycling voltammetry (CV) was conducted to compare the electrochemical properties of EGC with commercially available synthetic graphite,

Figure 1 shows the results of BN crystallization in molten $MgCl_2$ at 750 °C. The X-ray diffraction data shown in Figure 1a, amorphous BN shows no peaks indicative of a completely amorphous structure. After electrochemical treatment in the molten salt, the diffraction pattern manifests a characteristic peak observed at 2ϑ = 26°, representing the (002) plane, which confirms the transformation to h-BN.[13] The d_{002} value is calculated to be about 3.3 Å, consistent with previous literature.[13] Another smaller peak is observed at 2ϑ = 40°, representing the (100) and (101) plane. Further, h-BN synthesized at both -2.2 V and -2.6 V show a similar diffraction pattern. However, at higher cathodic potentials, peak intensity is observed to increase, suggesting higher crystallinity being achieved at -2.6 V versus -2.2 V. Finally, BN could not be crystallized in molten $CaCl_2$ even at higher temperatures (920 °C). Although a minor peak is observed near 2ϑ = 40°, the crystallization of BN in molten $CaCl_2$ appears to be very unfavorable. Hence, previously reported processes using molten $CaCl_2$ cannot be used for h-BN crystallization.[16] The reason for the inability of $CaCl_2$ to drive the crystallization is not clear and may need additional investigations.

SEM images of h-BN (Figure 1b, 1c, and S6) show flakes of h-BN indicative of an ordered structure compared to the disordered structure of amorphous BN (Figure S5). Careful analysis of the TEM images of h-BN (Figures 1d and S8) reveals an ordered, lattice-like structure compared to the disordered, amorphous structure of BN before treatment in the molten salt (Figure S7).

Compared to the previously reported process for the crystallization of h-BN, the electrochemical approach reported here is much simpler and safer. Previously, the synthesis of

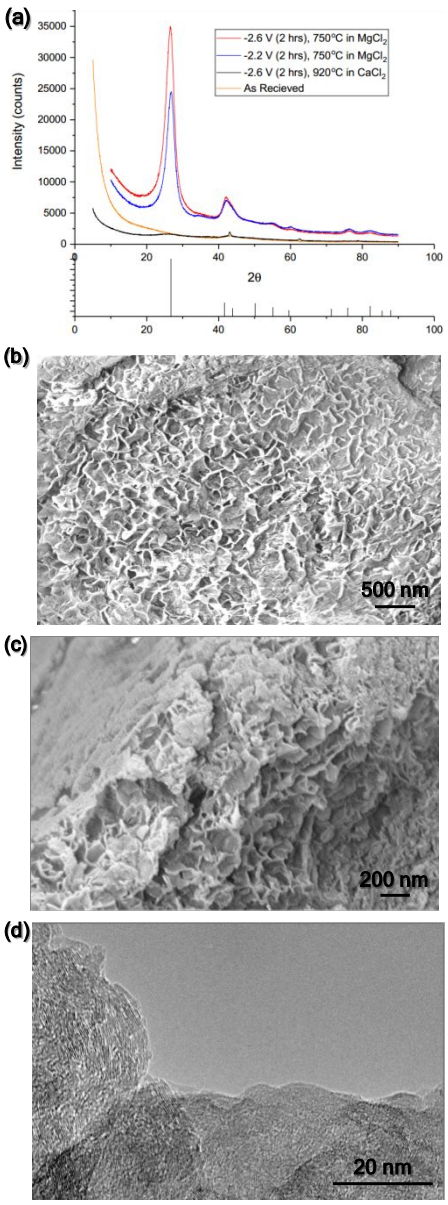

Fig. 1 (a) X-ray diffraction spectrum of the starting material (amorphous BN) compared to that of h-BN. (b)-(c) SEM images of h-BN showing flakes of BN (d) TEM image of h-BN showing an ordered crystal structure.

crystalline h-BN was reported at 900 °C using Mg metal,[13] the milder condition at 750 °C was achieved in this study. Further, the hazards associated with the handling of molten Mg metal are eliminated using the electrochemical approach here. Finally, as demonstrated here, it is possible to control the degree of crystallization by fine-tuning the applied voltage. This provides more flexibility and reaction control, which is not possible in the aforementioned process that simply employs Mg metal powder to catalyze the reaction. Since the BN is cathodically polarized, it is anticipated that Mg metal is generated in-situ at the cathode which scavenges oxygen impurities from the BN crystal structure which induces crystallization. This hypothesis is supported by previously proposed mechanisms in the analogous molten $CaCl_2$ system[16-20].

The analogous structural properties of BN and carbon led us to examine the application of molten $MgCl_2$ for graphite synthesis. To validate the versatility of the approach reported herein, amorphous carbon was graphitized at 810 °C. Attempts to graphitize amorphous carbon at 750 °C were unsuccessful, suggesting that a lower bound temperature for the synthesis of graphite. The amorphous carbon was cathodically polarized at -2.6 V for 2 hours. In Figure 2a, the X-ray diffraction spectrum of amorphous carbon and EGC is shown. Prior to treatment, amorphous carbon shows a broad peak indicating the amorphous state. After electrochemical treatment in the molten salt, a sharp, crystalline peak is observed at $2\vartheta = 26°$, which is characteristic of graphite. This result clearly indicates that molten $MgCl_2$ can be used for the transformation of hard, amorphous carbon to graphite.

TEM and SEM images of EGC shown in Figures 2b and 2c provide additional evidence of the graphitic morphology of EGC. TEM image clearly shows the layered structure of the carbon that is characteristic of graphite. Compared to the TEM of hard carbon shown in Figure S1, EGC shows a massively augmented layered structure. SEM image shows the flakes of graphite in comparison to the globular morphology of hard carbon shown in Figure S3. Holistic analysis of the XRD, SEM, and TEM data leads to the conclusion that the amorphous hard carbon was successfully transformed into graphite via cathodic polarization in molten $MgCl_2$ at 810 °C.

The feasibility of the EGC as an anode for fast charging battery applications was investigated. The electrochemical performance of EGC is shown in Figures 3a and 3b. The coin cells were galvanostatically cycled at three different rates (0.1 C, 1 C, and 5 C) to investigate the electrochemical performance at the high current rate and compare the result with state-of-the-art graphite. The EGC exhibits a first cycle discharge capacity of 685 mAh g^{-1}, well above the theoretical capacity (372 mAh g^{-1}) and first discharge capacity (348 mAh g^{-1}) of graphite (see Figure S9) and the first discharge capacity (418 mAh g^{-1}) of hard carbon (see Figure S10). The first-cycle coulombic efficiency for EGC is observed to be 40% comparable to hard carbon (46 %); however, lower than traditional graphite (81 %). The low first-cycle coulombic efficiency is likely due to the formation of the solid electrolyte interphase (SEI). Since the starting material has a high surface area (particle size 50 nm), more of the electrolyte is reacted to the surface leading to SEI formation.[21, 22] This phenomenon has been well documented in the literature previously.[23-25] Further, in the first cycle charge-discharge curves, an extended plateau is observed at around 0.8 V vs. Li/Li^+ and disappears after subsequent cycles, indicating that the formation of SEI takes place only during the first discharge cycle.[26-29] A comparison of the first discharge profile of EGCs with hard carbon and synthetic graphite reveals that EGC has a similar but extended plateau than hard carbon (see Figure S10), indicating that the porous nature of EGCs, which is beneficial for fast lithium diffusion kinetics. The first-discharge profile of synthetic graphite reveals a similar voltage plateau around 0.8 V, indicating the SEI formation, but much smaller than EGCs (see Figure S9). From the second cycle onwards, charge-discharge profiles of EGC resembles more like a graphitic behavior rather than to the hard carbon. These results were corroborated by the cyclic voltammetry experiment (see Figure S11). These results indicate that amorphous carbon was successfully graphitized. However, EGCs are not wholly graphitized as it still preserves the properties of the amorphous carbon, such as higher surface area and porosity verified by electrochemical data. The incomplete graphitization was carried out intentionally to tap the benefit of amorphous carbon such as higher surface area and porosity which led to fast lithium diffusion kinetics and graphitic backbone, which led to high energy density and stable cycling performances.

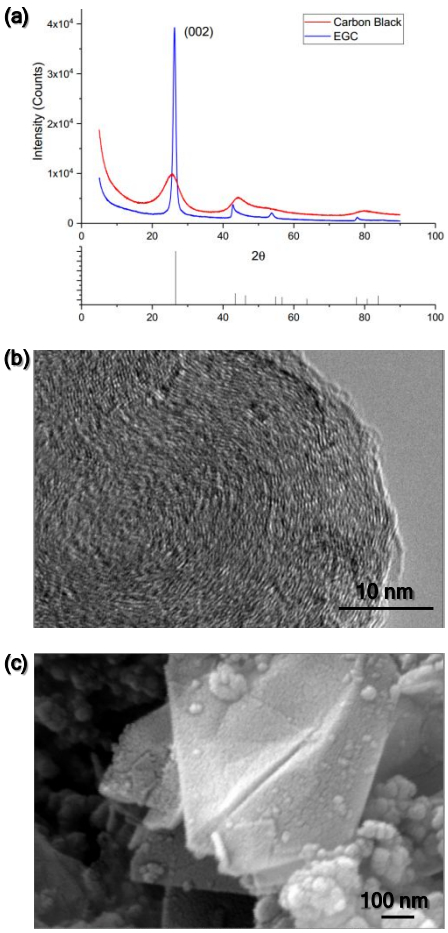

Fig. 2 (a) X-ray diffraction spectrum of the starting material (hard carbon) compared to that of EGC. (b) TEM images of EGC showing a layered structure characteristic of graphite. (c) SEM image of EGC showing flakes of graphite.

At 1 C and 5 C, a very stable capacity of about 200 mAh g^{-1} and 70 mAh g^{-1} at 99.9 % coulombic efficiency is observed for EGCs. This is much higher than the capacity of traditional graphite (25 mAh g^{-1}) (see Figure S9), which is consistent with previous literature.[30, 31] This much enhanced electrochemical performances of EGCs at higher charge-discharge rates signify the importance of the electrochemically driven graphitization comparing to the traditional graphite prepared from the thermal process. The stable higher capacity at fast charging indicates that EGCs could be used as an anode for the fast-charging battery. While the improvements in synthesis of graphite in molten $MgCl_2$ is only incremental in nature compared to previous research,[16] the synthesis of h-BN in molten $MgCl_2$ represents a

significant reduction in temperature and increased operational flexibility and process control.

In conclusion, herein, we report a novel process for the electrochemical transformation of amorphous BN to highly crystalline h-BN in molten $MgCl_2$ at 750 °C. This represents a significant reduction in temperature from previously reported literature. Additionally, the electrochemical approach reported here provides better operational control over the degree of graphitization. Further, the use of molten $MgCl_2$ for the synthesis of graphite has also been reported. The advances reported here are more modest. However, the electrochemical performances of EGC at high charge-discharge rates is much superior to the conventional battery grade anode graphite, indicating the economic importance of the process and possibility of EGCs being used as an anode for fast-charging energy storage devices.

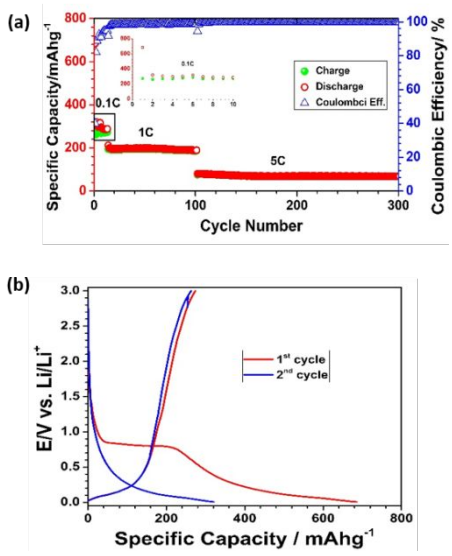

Fig. 3 (a) Battery performance of EGC at 0.1C, 1C, and 5C. EGC shows a capacity of about 70 mAh g^{-1}. (b) The charge-discharge profile for EGC shows a plateau at about 0.8 V vs. Li.

The research was funded by the Critical Materials Institute, an Energy Innovation Hub funded by the U.S. Department of Energy, Office of Energy Efficiency and Renewable Energy, Advanced Manufacturing Office.

Conflicts of interest

There are no conflicts to declare.

Notes and references

1. C. Tan, X. Cao, X.-J. Wu, Q. He, J. Yang, X. Zhang, J. Chen, W. Zhao, S. Han, G.-H. Nam, M. Sindoro and H. Zhang, *Chemical Reviews*, 2017, **117**, 6225-6331.
2. Q. Weng, X. Wang, X. Wang, Y. Bando and D. Golberg, *Chemical Society Reviews*, 2016, **45**, 3989-4012.
3. Q. Li, L. Chen, M. R. Gadinski, S. Zhang, G. Zhang, H. U. Li, E. Iagodkine, A. Haque, L.-Q. Chen, T. N. Jackson and Q. Wang, *Nature*, 2015, **523**, 576.
4. W. Zhu, Z. Wu, G. S. Foo, X. Gao, M. Zhou, B. Liu, G. M. Veith, P. Wu, K. L. Browning, H. N. Lee, H. Li, S. Dai and H. Zhu, *Nature Communications*, 2017, **8**, 15291.
5. P. Wu, S. Yang, W. Zhu, H. Li, Y. Chao, H. Zhu, H. Li and S. Dai, *Small*, 2017, **13**, 1701857.
6. Y. Kubota, K. Watanabe, O. Tsuda and T. Taniguchi, *Science*, 2007, **317**, 932-934.
7. T. Hagio, K. Nonaka and T. Sato, *Journal of materials science letters*, 1997, **16**, 795-798.
8. T. Hagio and H. Yoshida, *Journal of materials science letters*, 1994, **13**, 653-655.
9. S. Chen, R. Xu, J. Liu, X. Zou, L. Qiu, F. Kang, B. Liu and H. M. Cheng, *Advanced Materials*, 2019, **31**, 1804810.
10. A. Pakdel, Y. Bando and D. Golberg, *Chemical Society Reviews*, 2014, **43**, 934-959.
11. J. Yin, J. Li, Y. Hang, J. Yu, G. Tai, X. Li, Z. Zhang and W. Guo, *Small*, 2016, **12**, 2942-2968.
12. W. Zhu, X. Gao, Q. Li, H. Li, Y. Chao, M. Li, S. M. Mahurin, H. Li, H. Zhu and S. Dai, *Angewandte Chemie International Edition*, 2016, **55**, 10766-10770.
13. H. Chen, Z. Yang, Z. Zhang, Z. Chen, M. Chi, S. Wang, J. Fu and S. Dai, *Angewandte Chemie International Edition*, 2019, **58**, 10626-10630.
14. M. Ma, D. Wang, W. Wang, X. Hu, X. Jin and G. Z. Chen, *Journal Of Alloys and Compounds*, 2006, **420**, 37-45.
15. Z. Feng, X. Jiang, Y. Zhou, C. Xia, X. Zhang, M. Ma and R. Liu, *Prog. nat. sci. mater. Int.*, 2015, **25**, 496-502.
16. J. Peng, N. Chen, R. He, Z. Wang, S. Dai and X. Jin, *Angewandte Chemie International Edition*, 2017, **129**, 1777-1781.
17. K. Mohandas and D. Fray, *Trans. Indian Inst. Met*, 2004, **57**, 579-592.
18. R. Bhagat, M. Jackson, D. Inman and R. Dashwood, *Journal of The Electrochemical Society*, 2008, **155**, E63-E69.
19. M. Iizuka, T. Inoue, M. Ougier and J.-P. Glatz, *Journal of nuclear science and technology*, 2007, **44**, 801-813.
20. Y. Sakamura, M. Kurata and T. Inoue, *Journal of The Electrochemical Society*, 2006, **153**, D31-D39.
21. W. Luo, C. Bommier, Z. Jian, X. Li, R. Carter, S. Vail, Y. Lu, J.-J. Lee and X. Ji, *ACS Applied Materials & Interfaces*, 2015, **7**, 2626-2631.
22. C. J. Jafta, X.-G. Sun, G. M. Veith, G. V. Jensen, S. M. Mahurin, M. P. Paranthaman, S. Dai and C. A. Bridges, *Energy & Environmental Science*, 2019, **12**, 1866-1877.
23. E. Peled, C. Menachem, D. Bar‐Tow and A. Melman, *Journal Of The Electrochemical Society*, 1996, **143**, L4-L7.
24. S. S. Zhang, K. Xu and T. R. Jow, *Electrochimica Acta*, 2006, **51**, 1636-1640.
25. V. A. Agubra and J. W. Fergus, *Journal Of Power Sources*, 2014, **268**, 153-162.
26. J. Liu, S. Tang, Y. Lu, G. Cai, S. Liang, W. Wang and X. Chen, *Energy Environ. Sci.*, 2013, **6**, 2691-2697.
27. M. J. Jing, H. S. Hou, Y. C. Yang, Y. Zhang, X. M. Yang, Q. Y. Chen and X. B. Ji, *Electrochim. Acta*, 2015, **155**, 157-163.
28. H. Zhang, G. Cao, Z. Wang, Y. Yang, Z. Shi and Z. Gu, *Nano Lett.*, 2008, **8**, 2664-2668.
29. N. Palaniyandy, F. P. Nkosi, K. Raju and K. I. Ozoemena, *Mater. Chem. Phys.*, 2018, **209**, 65-75.
30. B. Guo, X. Wang, P. F. Fulvio, M. Chi, S. M. Mahurin, X.-G. Sun and S. Dai, *Advanced Materials*, 2011, **23**, 4661-4666.
31. F. Ding, W. Xu, D. Choi, W. Wang, X. Li, M. H. Engelhard, X. Chen, Z. Yang and J.-G. Zhang, *Journal Of Materials Chemistry*, 2012, **22**, 12745-12751.

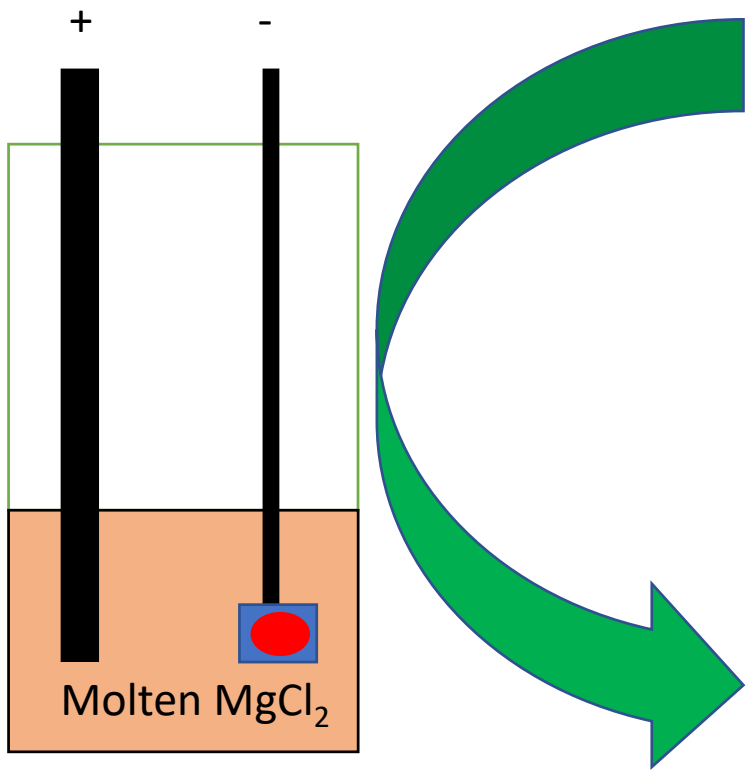

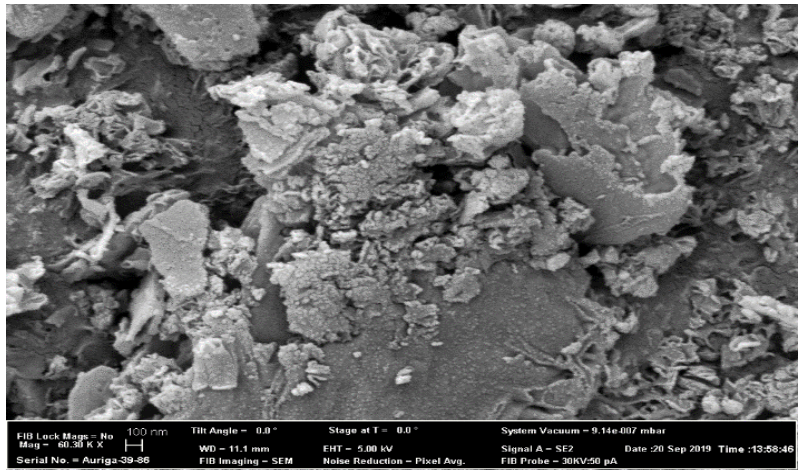

Amorphous Boron Nitride precursor

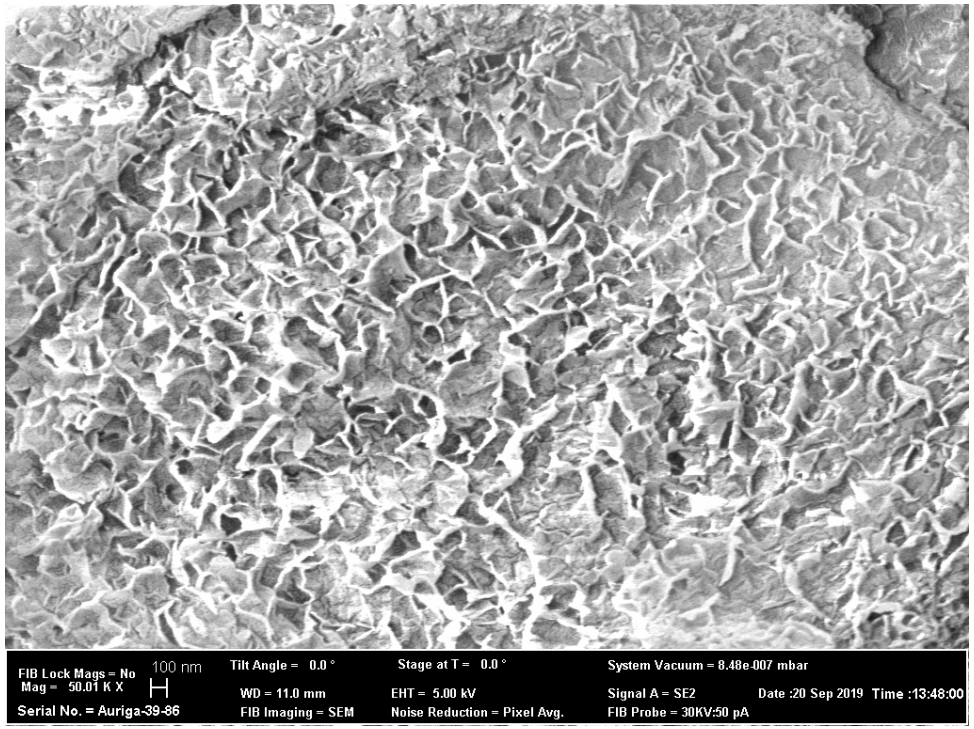

Crystalline hexagonal Boron Nitride